Ablation of Hypoxic Tumors with Dose-Equivalent Photothermal, but Not Photodynamic, Therapy Using a Nanostructured Porphyrin Assembly

Cheng S. Jin,[†,‡,§] Jonathan F. Lovell,[§,⊥] Juan Chen,[†] and Gang Zheng[†,‡,§,∥,*]

[†]Ontario Cancer Institute, Campbell Family Cancer Research Institute and Techna Institute, University Health Network (UHN), Toronto, Canada M5G 2M9, [‡]Department of Pharmaceutical Sciences, Leslie Dan Faculty of Pharmacy, University of Toronto, Toronto, Canada M5S 3M2, [§]Institute of Biomaterials and Biomedical Engineering, University of Toronto, Toronto, Canada M5S 1A1, [⊥]Department of Biomedical Engineering, University at Buffalo, State University of New York, Buffalo, New York 14260-2050, United States, and [∥]Department of Medical Biophysics, University of Toronto, Toronto, Canada M5G 1L7

ABSTRACT Tumor hypoxia is increasingly being recognized as a characteristic feature of solid tumors and significantly complicates many treatments based on radio-, chemo-, and phototherapies. While photodynamic therapy (PDT) is based on photosensitizer interactions with diffused oxygen, photothermal therapy (PTT) has emerged as a new phototherapy that is predicted to be independent of oxygen levels within tumors. It has been challenging to meaningfully compare these two modalities due to differences in contrast agents and irradiation parameters, and no comparative *in vivo* studies have been performed until now. Here, by making use of recently developed nanostructured self-quenched porphysome nanoparticles, we were able to directly compare PDT and PTT using matched light doses and matched porphyrin photosensitizer doses (with the photosensitizer being effective for either PTT or PDT based on the existence of nanostructure or not). Therefore, we demonstrated the nanostructure-driven conversion from the PDT singlet oxygen generating mechanism of porphyrin to a completely thermal mechanism, ideal for PTT enhancement. Using a novel hypoxia tumor model, we determined that nanostructured porphyrin PTT enhancers are advantageous to overcome hypoxic conditions to achieve effective ablation of solid tumors.

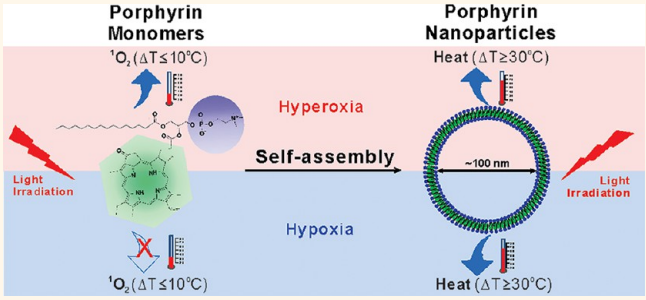

KEYWORDS: tumor hypoxia · nanoparticle · photothermal therapy · photodynamic therapy · porphyrin · porphysome

Tumor hypoxia, the condition in which tumor cells persist in a low oxygen environment, is a common feature of solid tumors. It poses a major therapeutic problem, as hypoxia-induced cellular changes can result in more clinically aggressive phenotypes,[1−5] and moreover, the reduced partial O_2 pressure in tumor tissue creates an obstacle for numerous cancer therapies, including ionizing radiotherapy,[6,7] certain types of chemotherapy,[7−9] and photodynamic therapy (PDT).[10,11]

PDT is a form of phototherapy that uses photosensitizers that are exposed selectively to light, whereupon they produce highly reactive oxygen species through either type I or type II reactions,[12,13] resulting in toxicity to targeted tissues. Classical PDT mostly follows the type II mechanism with porphyrin or porphyrin analogues often used as photosensitizers, among which Photofrin remains the gold standard PDT agent in clinical practice.[14] Thus, PDT requires synchronizing interactions among light, photosensitizers, and oxygen to be effective.[15] However, the oxygen-dependent nature of PDT limits its effectiveness in hypoxic tumors, and when partial oxygen pressure (pO_2) is below 40 mmHg, PDT efficacy decreases.[10,16,17] In addition, both photosensitizer-mediated oxygen consumption and blood vessel damage during PDT further potentiate tumor hypoxia, impeding therapeutic outcomes.[10,12,18,19] Thus, an oxygen-independent phototherapy such as photothermal therapy (PTT) could be a useful alternative for treating hypoxic tumors. Upon selective light treatment, instead of production of reactive

* Address correspondence to gang.zheng@uhnres.utoronto.ca.

Received for review December 19, 2012 and accepted February 10, 2013.

Published online February 11, 2013
10.1021/nn3058642

oxygen species, PTT agents absorb light and dissipate the absorbed energy through nonradiative decay (heating), which induces a temperature increase in the local treatment environment resulting in irreversible cell damage.[20,21]

Many light-absorbing species have been investigated as effective PTT agents. Most of the PTT agents developed to date are based on inorganic nanomaterials including gold nanoparticles (*e.g.*, nanocages,[22−24] nanorods,[25,26] nanoshells,[27,28] nanospheres[29,30]) and carbon nanotubes.[31−34] They are efficient in photon-to-thermal conversion due to the surface plasmon resonance (SPR) oscillation and high absorption cross section of NIR light.[35,36] Many chromophores have also been developed as PTT agents since the 1980s,[37] such as endogenous chromophores in tissue[38−40] externally added dyes such as indocyanine green,[41,42] naphthalocyanine,[43,44] and transition-metal-coordinated porphyrins.[37,45] However, PTT capability of monomeric chromophores is limited by their relatively low light absorption ($\varepsilon = 10^4-10^6\ M^{-1}\ cm^{-1}$) compared to gold nanoparticles with extinction coefficients orders of magnitude higher ($\varepsilon = 10^9-10^{11}\ M^{-1}\ cm^{-1}$).[36,44,46] Porphyrins have also been conjugated to gold nanoparticles or carbon nanotubes for enhanced light energy conversion and combination of photodynamic and photothermal therapy,[47−49] but only recently, porphyrin-based nanoparticles, termed porphysomes, have been developed to be the first organic PTT agents with comparable optical absoprtions to gold nanoparticles for high photothermal efficiency.[50] The liposomal nanostructure of porphyrin lipids provides additional advantages over inorganic PTT agents such as biocompatibility and biodegradability.[51]

Porphysomes are self-assembled from porphyrin lipid into liposome-like nanoparticles (~100 nm diameter). The porphyrin packing density per particle is high (>80 000 per particle), so they absorb light with extremely high efficiency. As the packing density also induced highly self-quenching porphyrin excited states, the absorbed energy is released as heat, providing exceptional properties as PTT agents. Therefore, unlike monomeric porphyrins, the unique nanoassembly of porphyrin lipids results in the conversion of the porphyrin photosensitizers from a singlet oxygen generating mechanism, useful for PDT, to a thermal mechanism, ideal for PTT enhancement. This creates a unique opportunity for the first time to compare, *in vivo*, the conversion of porphyrins from PDT photosensitizers to PTT transducers, by comparing porphyrin monomers to porphyrin nanoparticles.

In this study, we evaluated the nanostructure-driven conversion of the mechanism of PDT activation of porphyrin to PTT activation by *in vivo* studies, comparing the PDT and PTT efficacy of porphysomes in treating hyperoxic and hypoxic tumors. For the first time, we compared PTT to PDT directly in an *in vivo* hypoxic tumor model to investigate the advantages of PTT for treatment of hypoxic tumors. The study rationale and design are schematically illustrated in Figure 1.

RESULTS

Acute Hyperoxia and Hypoxia. We developed a multipronged approach to generate tumor hypoxia and hyperoxia *in vivo*. In general, partial oxygen pressure (pO_2) of the tumor could be modified by exposing mice to different inhalation concentrations of O_2. To investigate PDT and PTT in tumor hyperoxia and hypoxia conditions, mice were provided inhaled oxygen concentrations of 100 and 7%, respectively, prior to and during laser irradiation (Figure 2a). To further generate acute hypoxia conditions, a tourniquet was clamped onto one leg bearing a xenograft tumor in conjunction with 7% O_2 to ensure low oxygen levels at the tumor. Mice under hyperoxia conditions behaved normally during inspiration of 100% oxygen for 30 min. Their arterial partial oxygen pressure was 513.2 ± 67.1 mmHg (Figure S1 in Supporting Information), and hemoglobin was highly saturated with O_2 measured by photoacoustic (PA) imaging to be 99.9 ± 0% (Figure 2b and Figure S2 in Supporting Information). Mice in the hypoxia group breathing 7% O_2 exhibited a faster breathing rate and reduced movement. Partial oxygen pressure in artery blood circulation was reduced to 37.0 ± 4.3 mmHg (Figure S1 in Supporting Information). In addition, real-time PA imaging showed that the arterial oxyhemoglobin saturation rate of the mice decreased rapidly in the first 10 s upon exposure to 7% oxygen, reaching 75% after 1 min. Low oxygen conditions were maintained, and the arterial oxyhemoglobin saturation rate was kept around 74.7 ± 3.4% during the following 30 min using hypoxic gas exposure together with the leg tourniquet (Figure 2b and Figure S2 in Supporting Information). We further evaluated hypoxic conditions in the tumor by HIF-1α staining assay. HIF-1α is a heterodimeric transcription factor that plays a critical role in the cellular response to hypoxia.[52] As shown in Figure 2c, the nuclei of tumor cells of the hypoxia group stained dark brown, indicating the nuclear accumulation of HIF-1α under hypoxic conditions, while the nuclei of hyperoxic tumor cells remained blue, indicating HIF-1α was not detected. Both the *in vivo* measurement of partial oxygen pressure arterial oxyhemoglobin saturation rate and *ex vivo* HIF-1α staining confirmed that, by combining controlled inhalation gases (100 or 7% oxygen) together with tourniquet-based blood restriction, biologically relevant acute hyperoxic and hypoxic tumor conditions could be generated.

Drug Dark Toxicity. To keep the drug accumulation consistent for treatment in hyperoxic and hypoxic conditions, Photofrin or porphysomes were both matched at 10 mg/kg porphyrin dose and were intravenously injected into mice bearing KB tumors in a

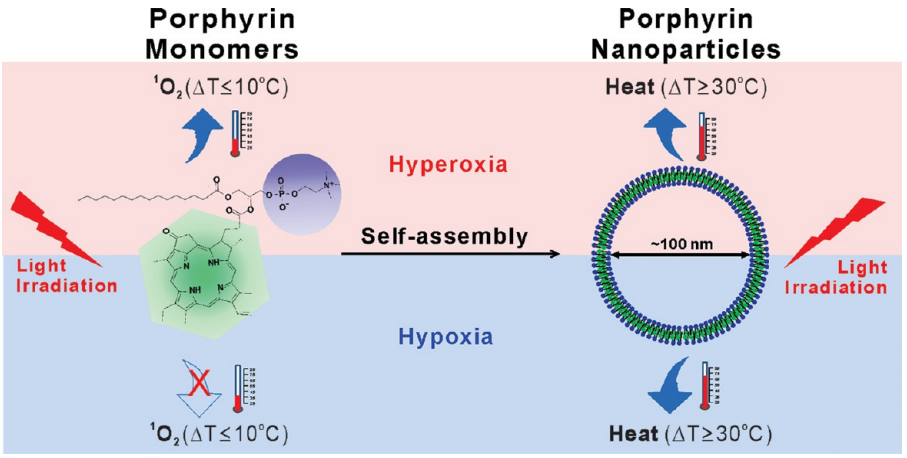

Figure 1. Schematic illustration of the study rationale and design.

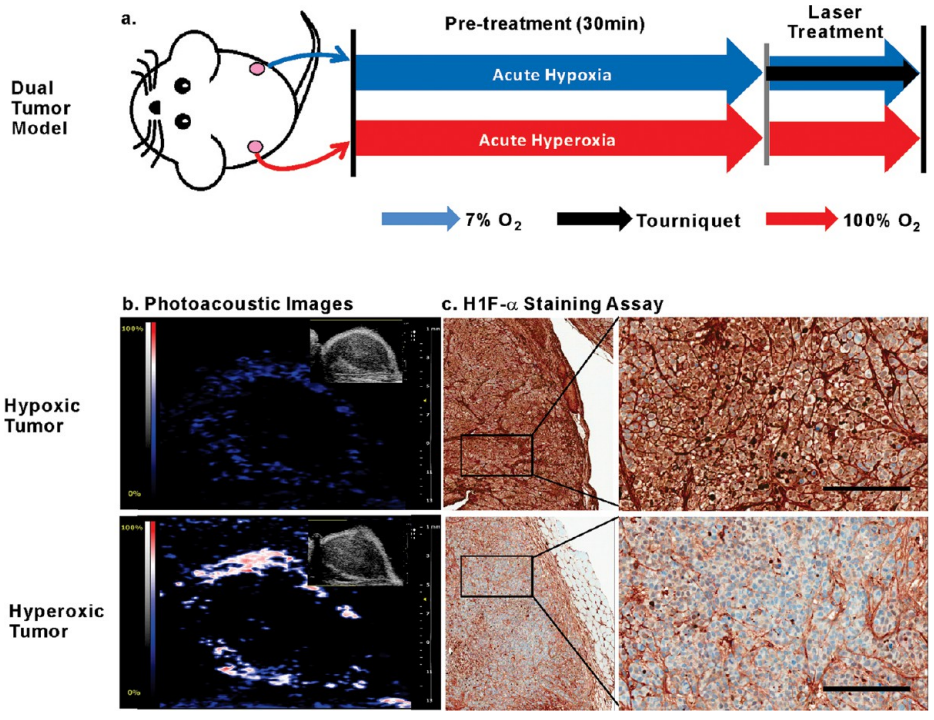

Figure 2. Development of dual hyperoxia/hypoxia tumor model in a single mouse, with confirmation of hypoxia by photoacoustic imaging and HIF-1α staining assay. (a) Generation of acute hypoxia/hyperoxia; (b) photoacoustic microscope of the map of hemoglobin oxygen saturation (sO_2) of KB xenograft on mouse flank *in vivo*; and (c) *ex vivo* HIF-1α staining. Scale bar: 200 μm.

normal air environment. Twenty-four hours post-injection, mice were then exposed to either hyperoxic or hypoxic conditions for PDT/PTT treatment. The tumor size of the mice was controlled to be less than 5 mm to minimize the confounding influences of intrinsic tumor necrosis and hypoxia. Corresponding H&E staining did not show any morphological change compared to control xenografts, demonstrating that no obvious dark toxicity was induced by these two agents (Figure S3 in Supporting Information).

Treatment Response. To compare PDT and PTT in hyperoxic and hypoxic conditions, a treatment study was designed, as shown in Table 1, and included three groups of experiments: Photofrin for PDT, porphysomes for PDT, and porphysomes for PTT. Both Photofrin and porphysomes were injected intravenously (i.v.) into mice bearing dual xenograft tumors at each rear leg at a dose of 10 mg/kg porphyrin content. Although i.v. porphyrin injected doses were kept the same, comparing Photofrin PDT directly to porphysome PTT does not account for possible confounding factors such as differences in photophysical properties of the porphyrin and the laser (635 nm *vs* 671 nm), as well as expected differences in porphyrin biodistribution. Therefore, we developed a more meaningful comparison system by developing a novel single mouse—dual

TABLE 1. Design of the Comparison between Porphyrin Molecules and Porphyrin Self-Assembled Nanoparticles with Matched Light Doses and Matched Photosensitizer Doses

	Photofrin	porphysomes	
structure	heterogeneous small molecule, mixture of porphyrin monomers, dimers, and oligomers[12]	porphyrin self-assembled nanovesicles[50] (~100 nm)	
porphyrin dose	10 mg/kg		
Wavelength	635 nm	671 nm	
light power	200 mW (PDT)	200 mW (PDT)	750 mW (PTT)
light dose	100 J/cm^2		
oxygen level	hyperoxia/hypoxia		

tumor model, where biodistribution of the therapeutic agent was similar in both tumors, but one of the two tumors had hypoxia effectively induced prior to treatment. The left tumor was used to conduct PDT/PTT treatment under hyperoxic conditions, and the right tumor was used for hypoxic conditions (Figure 2a).

The thermal effect of Photofrin and porphysomes during PDT and PTT irradiation, as well as laser-only controls, was evaluated by monitoring tumor temperature during treatment. Laser-only controls (including three laser settings: 635 nm at 200 mW, 671 nm at 200 mW, and 671 nm at 750 mW) caused a mild temperature increase (<6 °C, Figure S4 in Supporting Information), and even the high-power laser (671 nm, 750 mW) did not induce tumor growth inhibition that had been demonstrated in previous porphysome papers.[50,51] Photofrin combined with its PDT laser (635 nm at 200 mW) caused a slow and continuous temperature increase to 36.2 ± 1.7 °C in hyperoxic tumors and 39.2 ± 1.2 °C in hypoxic tumors at the end of the 5 min treatment (Figure 3). Similarly, porphysome combined with PDT laser conditions (671 nm at 200 mW) induced a mild temperature increase to a final temperature of 43.3 ± 1.5 °C in a hyperoxic tumor and 42.3 ± 1.1 °C in hypoxic tumors (Figure 3). However, in porphysome PTT treatment (671 nm at 750 mW for 85 s—an equivalent laser energy), the temperature of hyperoxic and hypoxic tumors increased to 65.5 ± 2.0 and 67.1 ± 5.5 °C, respectively, demonstrating an effective photothermal response of porphysome for both hyperoxic and hypoxic tumors (Figure 3). For each type of phototherapy, the difference between final temperatures of hypoxic and hyperoxic tumors was not significant based on *t* test, indicating that heat generation along laser irradiation was not dependent on local oxygen level. In addition, HIF-1α staining of hyperoxic tumor tissues was also conducted after Photofrin/porphysome PDT irradiation (Figure S5 in Supporting Information). Compared to the control hyperoxic tumor without laser irradiation (Figure S5a), the majority of tumor cells with Photofrin PDT treatment have been stained dark at nuclei (Figure S5b), indicating the lack of oxygen post-PDT treatment, while nuclei of post-porphysome PDT tumor cells mainly stayed unchanged (Figure S5c).

To evaluate treatment efficacy, H&E staining of tumor tissue after PDT or PTT treatment was conducted. An untreated hyperoxic tumor and a hypoxic tumor were used as controls (Figure 4a), and no necrosis or obvious apoptosis was observed in these samples. The tumor that received Photofrin PDT under hyperoxic conditions showed signs of cell destruction and extensively damaged areas, including the loss of tissue architecture and decreased general intensity of tissue (Figure 4b). However, the tumor remained unaffected when Photofrin PDT was conducted under hypoxic conditions (Figure 4b). These data show that PDT efficacy occurred with sufficient oxygen supply in the tumor but not when the oxygen level was reduced to hypoxic levels.

Following administration of porphysomes, the tumors irradiated under PDT conditions (671 nm, 200 mW, 5 min 18 s) did not show tissue or cellular damage under either hyperoxia or hypoxia conditions, which indicated porphysomes were ineffective PDT regardless of intratumor oxygen level (Figure 4c). In contrast, porphyrin and laser-dose-equivalent porphysome PTT (671 nm, 750 mW, 85 s) induced great temperature increase in both hyperoxic and hypoxic tumors very rapidly (ΔT > 30 °C and T_{final} > 60 °C). This caused widespread tumor bleaching and obvious tissue damage at 24 h post-PTT, with severe morphological changes induced in tumor cells in both hyperoxic and hypoxic tumors (Figure 4d).

Tumor Growth and Survival Study. A tumor growth and survival study was conducted (Figures 5 and 6). For the hyperoxic group treated with Photofrin PDT, dark brown ablation spots were observed at tumor areas starting from day 2 post-treatment (Figure 5a), and the tissues slowly recovered in the following two weeks with 100% survival rate (Figures 5b and 6). For the hypoxic group that received Photofrin PDT, no obvious tumor ablation was observed (Figure 5a) and tumors continued to grow and reached the end point starting at day 4 post-treatment, and all mice reached end point by day 19 (Figures 5b and 6). For the mice treated with porphysome PDT, both hyperoxic and hypoxic tumors appeared unaffected and continued to grow (Figures 5b and 6). The mice received PDT under hypoxia conditions started to reach end point on day 6, and all mice were sacrificed by day 8. Growth of the tumor that received PDT under hyperoxia conditions occurred slightly slower than that of the hypoxic group

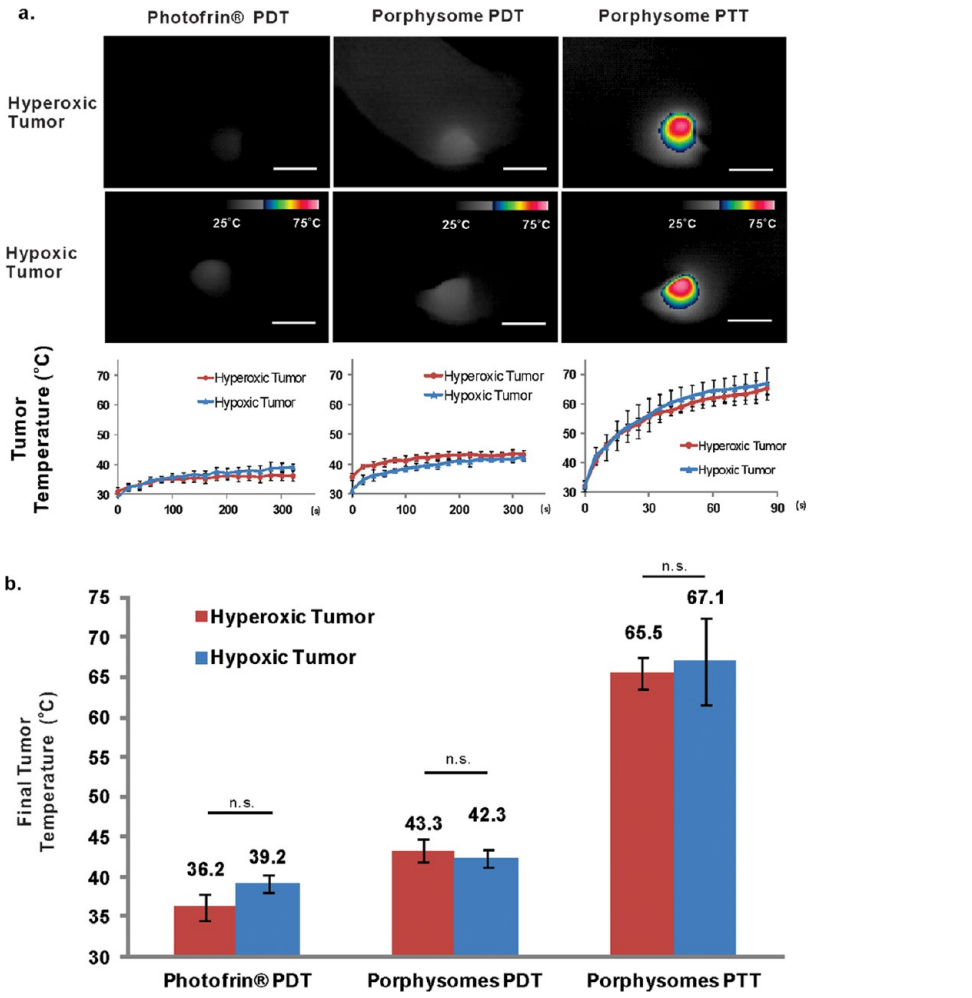

Figure 3. Temperature increase upon laser irradiation: Photofrin PDT, porphysome PDT, and porphysome PTT. (a) Heat map captured by thermal camera in hyperoxic and hypoxic tumors subjected to various irradiations (scale bar: 8 mm), and temperature increase curves of tumors measured by a thermal camera. (b) Final tumor temperatures after laser irradiation. Data expressed as mean ± SD (n = 5), and "n.s." indicates $p > 0.05$.

(not statistically significant) and reached the end point by day 8, as well. The tumors in both hyperoxic and hypoxic conditions were ablated by the heat following porphysome PTT, and eschars were observed on day 2 and recovered within two weeks. The hyperoxic group achieved 100% survival rate, and the hypoxia group achieved 80% survival. The lower survival rate in the hypoxic group was not due to inefficient PTT treatment at hypoxia condition but was because one of the five mice in hypoxic group had a distant tumor which was not covered by PTT laser irradiation (Figures 5b and 6).

DISCUSSION

Phototherapies including photodynamic therapy (PDT) and photothermal therapy (PTT) are presently being investigated and developed as alternatives to conventional cancer treatment modalities.[13,36] Both therapies are minimally invasive in nature, have high selectivity (localized laser irradiation) and relative simple performance which can lead to improved recovery times, reduce the risk of complications, and treat embedded tumors in microsurgeries.[13,53] Both PDT and PTT involve the administration of light-absorbing molecules, followed by laser activation of specific wavelength in the visible or near-infrared (NIR) region, but they differ in the laser intensity requirement for different energy-transducing mechanisms.[13,36] PDT is highly dependent on molecular oxygen for sufficient singlet oxygen production, while PTT, relying on the physical process of heating, is an alternative phototherapy that remains effective even under hypoxia conditions, and the advantage of PTT in treating hypoxic tumor cells was previously verified by *in vitro* cell study.[54]

Porphyrins are the most commonly used PDT sensitizers, but the unique nanostructure self-assembled from porphyrin–lipid conjugates (porphysomes) results in the conversion from PDT utility into potent PTT agents. To the best of our knowledge, this is the first study comparing the PDT and PTT efficacies in treating hypoxic tumors in *in vivo* studies. Porphysome PTT clearly achieved the best overall efficacy in treating

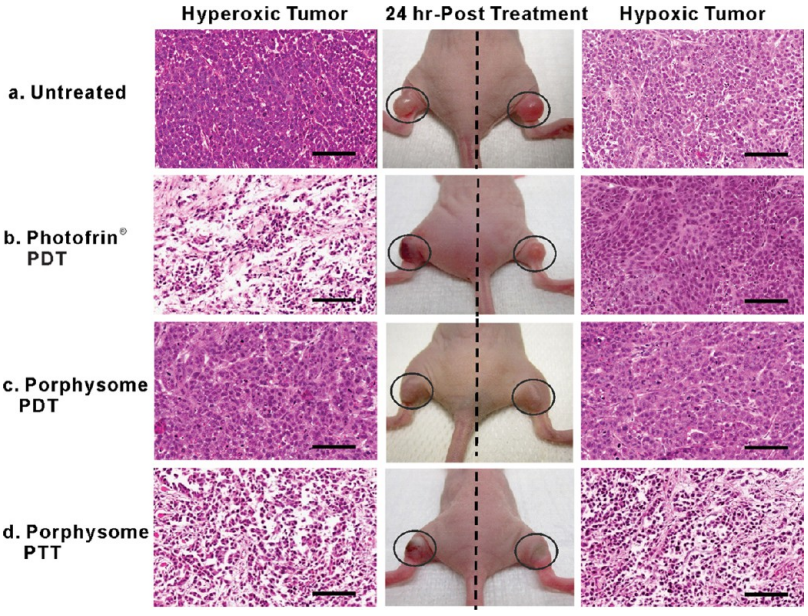

Figure 4. Tumors at 24 h post-treatment and corresponding H&E staining of tumor slides: (a) tumor controls without any injection or light illumination; (b) tumors with Photofrin (10 mg/kg) injected and underwent Photofrin PDT laser (200 mW); (c) tumors with porphysomes (10 mg/kg) injected and irradiated by porphysome PDT laser (200 mW); (d) tumors with porphysomes (10 mg/kg) injected and irradiated by PTT laser (750 mW). Scale bar: 100 μm.

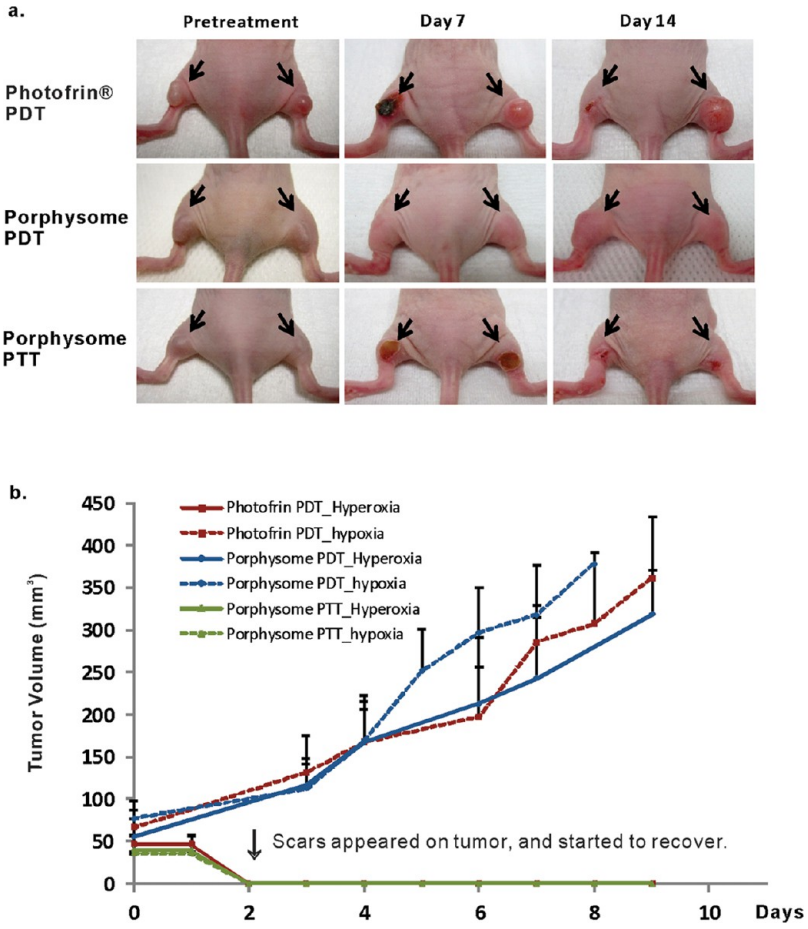

Figure 5. (a) Therapeutic response to photodynamic therapy by Photofrin or porphysomes and photothermal therapy using porphysomes pre- and post-treatment ($n = 5$). (b) Tumor growth in each laser irradiation group. Data expressed as mean $\pm$ SD ($n = 5$).

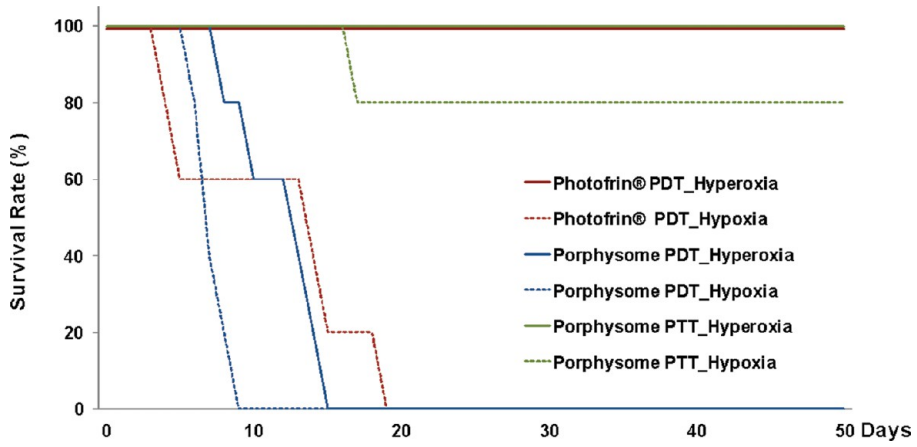

Figure 6. Survival study following each laser irradiation. Mice were sacrificed when tumor reached 10 mm diameter (n = 5).

both hyperoxic and hypoxic tumors since both Photofrin PDT and porphysome PDT were not therapeutically active in hypoxic conditions.

In this study, we focused on the essential role of O_2 in effective laser therapy, so the animal model was designed with the following in mind: (1) small tumors were used with size not exceeding 5 mm diameter to avoid self-necrosis and intrinsic hypoxia; and (2) both hyperoxia and hypoxia were generated as acute conditions 24 h after Photofrin or porphysomes were administered but before the laser treatment to ensure the same tumor accumulation under these two different oxygen levels. Therefore, we were able to simplify the investigation and study the influence of oxygen, as the only variable, on the therapeutic efficacy of PDT and PTT by avoiding the adverse effects of intrinsic hypoxia on drug biodistribution and cellular physiological functions.

As a commercial gold standard PDT agent, Photofrin was effective in treating mice bearing KB xenograft under hyperoxic conditions (100% reduction in tumor volume 2 days after treatment and 100% survival over 50 days). PDT therapeutic efficacy of porphyrins was eliminated when they were assembled as lipid conjugates in the bilayer of self-quenched porphysome nanoparticles. The extremely high density of porphyrin leads to a static-quenching property, during which fluorescence and singlet oxygen production is both inhibited, and the absorbed light energy is mainly dissipated as heat with extinction coefficients as high as gold nanorods.[50] Therefore, due to the unique nanostructure of self-assembled porphyrin–lipid conjugates, intact porphysomes functioned as potent photothermal enhancers that induced rapid and significant tumor temperature increase (T_{final} > 60 °C in 85 s) upon PTT irradiation for a complete tumor elimination regardless of cellular oxygen amount at both hyperoxic and hypoxic conditions.

The nanostructure of self-assembled porphyrin–lipid conjugates resulted in more stable and extremely high density of porphyrin, compared to conventional liposomal delivery systems where free porphyrin are inserted into either the core or lipid bilayer of the liposome. Previous studies have demonstrated that porphysomes have a good *in vivo* half-life of 12 h for i.v. administration, and they are able to take advantage of the enhanced permeability and retention (EPR) effect to achieve an excellent tumor accumulation of 7.5% ID/g 24 h post-injection.[50,51] Therefore, the nanoscale structure also helped to achieve good pharmacokinetic properties, such as prolonged circulation time and high tumor biodistribution.

This study provides direct evidence that oxygen is a crucial component in successful porphyrin PDT treatment *in vivo*. Photofrin PDT was effective in treating hyperoxic tumors (100% reduction in tumor volume 2 days after treatment and 100% survival over 50 days) but not hypoxic tumors (no tumor cell damage, no tumor growth suppression compared to untreated group, and no survival after 20 days) (Figures 4–6). In contrast, porphysome-enabled PTT was effective against both hyperoxic and hypoxic tumors. Typically, PTT aims to heat tumors to 50–55 °C because cellular death occurs at that temperature range.[21,55] In this study, the dose-equivalent injected porphysomes consisting of porphyrin dose at 10 mg/kg were able to generate heat upon PTT laser irradiation (PDT energy equivalent) to a final tumor temperature higher than 60 °C in both hyperoxic and hypoxic tumors in a period of only 85 s (Figure 3) and thus cured the tumor completely without recurrence. These results indicate that engineering nanostructured self-assemblies has practical implications in overcoming physiological obstacles in cancer therapies such as hypoxic conditions by thermal ablation. In addition, in this study, we used laser irradiation conditions that resulted in either PDT (200 mW) or PTT (750 mW). It would be interesting, in future studies, to examine the effects of intermediate light doses in terms of therapeutic efficacy in differing oxygen conditions.

The unique structure and physiochemical properties of porphysomes make them a good candidate for

multimodal imaging, which can serve for diagnosis and therapy. Because the nanostructure enables the heat generation upon laser irradiation, porphysomes exhibit unique photoacoustic imaging besides PTT efficacy.[50] Additionally, despite the high level of fluorescence self-quenching when the structure is intact, porphysomes become partially unquenched upon tumor accumulation, permitting low background fluorescence imaging. Therefore, porphysomes are intrinsically suitable for fluorescence imaging because of the conjugated porphyrin. Besides, each porphyrin has a stable site for chelating radioisotopes; therefore, porphysomes can be easily labeled with radioisotopes such as ^{64}Cu for PET imaging.[56] Furthermore, the liposomal nanostructure of the porphysome provides the capability of porphysomes to carry therapeutic and imaging agents. All of the above characteristics relate to this porphyrin-based organic nanostructure and make porphysomes an attractive system for combinational therapy and multimodal image-guided therapy, which has potential to be developed for new treatment paradigms of hypoxic tumors.

CONCLUSION

The unique porphyrin-based self-assembled nanostructure (porphysome) enabled photothermal activation by the conversion of pyropheophorbide from a singlet oxygen generating mechanism, useful for PDT, to a completely thermal mechanism, ideal for PTT enhancement. The PTT therapeutic efficacy of porphysome nanotechnology offers a potential advantage and provides an alternative phototherapy of PDT to treat hypoxic tumor *in vivo*. In porphyrin dose and laser energy dose matched studies, only PTT was effective enough in treating hypoxic tumors. This unique property can presumably be extended to other PTT contrast agents, as well, such as gold nanoparticles, for treating hypoxic tumors.

METHODS

Animal Preparation and Tumor Model. All animal experiments were performed in compliance with University Health Network guidelines. The animal studies were conducted on nude mice with KB xenografts. Nu/nu nude female mice were purchased from Charles River and kept in the Animal Research Centre of University Health Network. KB cells were cultured in RPMI-1640 media with 10% FBS. KB cells (1×10^6) were inoculated subcutaneously in the nude mice, and the experiments were conducted approximately 2 weeks post-inoculation when the tumors attained a surface diameter of 4−5 mm with the volume around 30 mm^3.

Mice with dual tumors (Figure 1a) were used for post-treatment tumor monitoring ($n = 5$ per group) and H&E staining histology study ($n = 3$ per group). Mice with a single tumor were used for tumor growth measurement and survival studies ($n = 5$ per group).

Acute Hyperoxia and Hypoxia. Prior to PDT/PTT treatment, mice were given 100% oxygen for 30 min before the treatment and during PDT/PTT laser irradiation (Figure 2a). To simulate acute hypoxia, mice were placed in 7% oxygen (with 93% nitrogen) atmosphere for 30 min. Additionally, a tourniquet was placed on the leg bearing the xenograft with a clamp, together with 7% O_2 during the laser irradiation to further ensure the low oxygen level at tumor area (Figure 2a).

Photoacoustic Imaging. The hemoglobin oxygen saturation (sO_2) in the blood vessels at the tumor area was monitored using a preclinical photoacoustic (PA) imaging system (VevoLAZR, VisualSonic Inc., Toronto) under hyperoxic (100% O_2) and hypoxic (7% O_2) conditions. The same tumor was used to map the change of sO_2 at the tumor with different oxygen supplies by PA. The mouse tumor was imaged under hyperoxia first for 30 min, and the gas supply was then switched to 7% O_2 (with 93% N_2) for 30 min. The tourniquet method was performed for 5 min additionally to the 7% O_2 treatment at the end, and the oxygen saturation image was obtained again after the tourniquet method was given.

HIF-1α Staining. HIF-1α staining assay was used to confirm tumor hypoxia. Mice with KB xenografts in the hyperoxia group were treated by 100% O_2 for 30 min, and the mice of the hypoxia group were given 7% oxygen for 30 min and tourniquet method was performed for an additional 5 min. Mice were sacrificed at the end of the treatment, and tumors were harvested and fixed in 10% formaldehyde for HIF-1α staining.

Photofrin and Porphysome Preparation. Photofrin was purchased from AXCAN PHARMA (15 mg per vial, Quebec, Canada) and diluted in 5% dextrose to a concentration of 1 mg/mL for intravenous injections. Porphysomes were prepared in-house using previously described methods.[50] Briefly, a lipid film was prepared by combining 55 mol % of porphyrin lipid and 40 mol % of cholesterol (Avanti Polar Lipids), with 5 mol % of distearoylglycero-3-phosphoethanolamine-*N*-methoxy(polyethene glycol) (PEG-PE, Avanti Polar Lipids) dissolved in chloroform, and dried under a stream of nitrogen gas and further dried under vacuum for 1 h. The lipid film was stored at 20 °C under argon until rehydration with phosphate buffered saline (150 mM NaCl, 10 mM phosphate, pH 7.4) and was then subjected to five freeze−thaw cycles. The porphysome suspension was extruded 10 times using 10 mL of LIPEX Thermobarrel Extruder (catalogue# T.005, Northern Lipids Inc., CA) through a 100 nm pore size polycarbonate membrane (Avanti Polar Lipids) at 70 °C. Porphysomes were usually formed at 4 mg/mL, taken as the initial sum of all of the components. Porphysome concentration was assessed by measuring the absorption in methanol, using the molar extinction coefficients of 97 000 M^{-1} cm^{-1} at 410 nm for pyropheophorbide and assuming 83 000 porphyrin−lipid molecules per porphysome. Porphysome size was measured using a Malvern ZS90 Nanosizer (Malvern Instruments). Porphysomes solutions were diluted in buffered saline, three measurements were performed with 15 runs each, and the results were averaged. Both Photofrin and porphysome were freshly prepared and kept sterile prior to animal i.v. injection.

Photodynamic and Photothermal Laser Irradiation. The study was designed as shown in Table 1, including three groups of experiments: Photofrin with PDT irradiation, porphysomes with PDT irradiation, and porphysomes with PTT irradiation. Both Photofrin and porphysomes were injected i.v. into xenograft-bearing mice at a dose of 10 mg/kg, calculated on the porphyrin content.

Therapeutic Conditions. For Photofrin PDT, tumors were irradiated with a 633 nm laser (DPSS laser, LaserGlow Technologies, Toronto, Canada), and the power was measured as 200 mW with a spot size of 9 mm diameter for 318 s. For porphysome PDT, a 671 nm laser was used (DPSS laser, LaserGlow Technologies, Toronto, Canada) at an output of 200 mW with the spot size of 9 mm diameter for 318 s. For porphysome PTT, the output at 671 nm was adjusted to 750 mW with a spot size of 9 mm diameter for 85 s (DPSS laser, LaserGlow Technologies, Toronto, Canada). The total light dose was 100 J/cm^2 for each of Photofrin PDT, porphysome PDT, and porphysome PTT.

Temperature Monitoring. During each irradiation, tumor temperature was monitored using an infrared thermal camera (Mikroshot, LUMASENSE Technologies). The final tumor temperature was calculated with $n = 5$ in each treatment group for average and standard deviation.

Histology Study. To evaluate laser ablation induced by laser therapy, tumors (~4 mm diameter) were harvested for histology studies. Tumors that only underwent acute hyperoxia and hypoxia but no laser treatment were used as controls. For the tumor that received each of the six treatment combinations (3 types of phototherapy × 2 levels of oxygen conditions), the whole tumor was dissected 24 h after laser irradiation and fixed in 10% formaldehyde. Tumors were then sectioned into slices of 8 μm thickness, and H&E staining was carried out by standard methods at the Pathology Research Program Laboratory at University Health Network. The sections were viewed and photographed by bright-field microscopy at 20×.

Post-treatment Tumor Monitoring. Tumor growth was monitored after treatment by measuring the diameters with a Vernier caliper once every two days. The volume was calculated as $V = \pi/6 \times a \times b^2$. Mice were euthanized at the defined end point when tumor diameter reached 10 mm, and survival curve was plotted accordingly.

Statistical Analysis. The Student's *t* test (two-tailed) was used to determine the significance of the difference in tumor temperature and tumor volume between hyperoxic and hypoxic conditions in each phototherapy group.

Conflict of Interest: The authors declare no competing financial interest.

Acknowledgment. We thank Jiachuan Bu and Elizabeth Huynh for helping operating VevoLAZR Photoacoustic Imaging system, and Drs. Brian C. Wilson, Robert G. Bristow, K. Sandy Pang, and Parimal Nathwani for valuable discussion. This work was supported by grants from the MaRS Innovation, the Canadian Institute of Health Research, the Canadian Space Agency, the Prostate Cancer foundation of Canada, the Natural Sciences and Engineering Research Council of Canada, the Canadian Foundation for Innovation, the Princess Margaret Cancer Center Foundation, and the Joey and Toby Tanenbaum/Brazilian Ball Chair in Prostate Cancer Research.

Supporting Information Available: Measurement of partial oxygen pressure and hemoglobin oxygen saturation under acute hyperoxia and hypoxia conditions, Photofrin/porphysomes' *in vivo* dark toxicity study, heating curves of normal tissue control under each laser irradiation, as well as HIF-1α stained hyperoxic tumor slides before and after Photofrin/porphysome PDT treatment. This material is available free of charge *via* the Internet at http://pubs.acs.org.

REFERENCES AND NOTES

1. Hockel, M.; Schlenger, K.; Aral, B.; Mitze, M.; Schaffer, U.; Vaupel, P. Association between Tumor Hypoxia and Malignant Progression in Advanced Cancer of the Uterine Cervix. *Cancer Res.* **1996**, *56*, 4509–4515.
2. Brizel, D. M.; Scully, S. P.; Harrelson, J. M.; Layfield, L. J.; Bean, J. M.; Prosnitz, L. R.; Dewhirst, M. W. Tumor Oxygenation Predicts for the Likelihood of Distant Metastases in Human Soft Tissue Sarcoma. *Cancer Res.* **1996**, *56*, 941–943.
3. Sundfor, K.; Lyng, H.; Rofstad, E. K. Tumour Hypoxia and Vascular Density as Predictors of Metastasis in Squamous Cell Carcinoma of the Uterine Cervix. *Br. J. Cancer* **1998**, *78*, 822–827.
4. Hockel, M.; Schlenger, K.; Hockel, S.; Aral, B.; Schaffer, U.; Vaupel, P. Tumor Hypoxia in Pelvic Recurrences of Cervical Cancer. *Int. J. Cancer* **1998**, *79*, 365–369.
5. Walenta, S.; Wetterling, M.; Lehrke, M.; Schwickert, G.; Sundfor, K.; Rofstad, E. K.; Mueller-Klieser, W. High Lactate Levels Predict Likelihood of Metastases, Tumor Recurrence, and Restricted Patient Survival in Human Cervical Cancers. *Cancer Res.* **2000**, *60*, 916–921.
6. Bristow, R. G.; Hill, R. P. Molecular and Cellular Basis of Radiotherapy. In *The Basic Science of Oncology*, 4th ed.; The McGraw-Hill Companies, Inc.: New York, 2005; pp 261−288.
7. Durand, R. E. The Influence of Microenvironmental Factors during Cancer Therapy. *In Vivo* **1994**, *8*, 691–702.
8. Teicher, B. A.; Lazo, J. S.; Sartorelli, A. C. Classification of Antineoplastic Agents by Their Selective Toxicities toward Oxygenated and Hypoxic Tumor Cells. *Cancer Res.* **1981**, *41*, 73–81.
9. Teicher, B. A.; Holden, S. A.; Al-Achi, A.; Herman, T. S. Classification of Antineoplastic Treatments by Their Differential Toxicity toward Putative Oxygenated and Hypoxic Tumor Subpopulations *in Vivo* in the Fsaiic Murine Fibrosarcoma. *Cancer Res.* **1990**, *50*, 3339–3344.
10. Henderson, B. W.; Fingar, V. H. Relationship of Tumor Hypoxia and Response to Photodynamic Treatment in an Experimental Mouse Tumor. *Cancer Res.* **1987**, *47*, 3110–3114.
11. Vaupel, P.; Thews, O.; Hoeckel, M. Treatment Resistance of Solid Tumors: Role of Hypoxia and Anemia. *Med. Oncol.* **2001**, *18*, 243–259.
12. MacDonald, I. J.; Dougherty, D. J. Basic Principles of Photodynamic Therapy. *J. Porphyrins Phthalocyanines* **2001**, 105–129.
13. Wilson, B. C.; Patterson, M. S. The Physics, Biophysics and Technology of Photodynamic Therapy. *Phys. Med. Biol.* **2008**, *53*, R61–109.
14. O'Connor, A. E.; Gallagher, W. M.; Byrne, A. T. Porphyrin and Nonporphyrin Photosensitizers in Oncology: Preclinical and Clinical Advances in Photodynamic Therapy. *Photochem. Photobiol.* **2009**, *85*, 1053–1074.
15. Lovell, J. F.; Liu, T. W.; Chen, J.; Zheng, G. Activatable Photosensitizers for Imaging and Therapy. *Chem. Rev.* **2010**, *110*, 2839–2857.
16. Lee See, K.; Forbes, I. J.; Betts, W. H. Oxygen Dependency of Photocytotoxicity with Haematoporphyrin Derivative. *Photochem. Photobiol.* **1984**, *39*, 631–634.
17. Mitchell, J. B.; McPherson, S.; DeGraff, W.; Gamson, J.; Zabell, A.; Russo, A. Oxygen Dependence of Hematoporphyrin Derivative-Induced Photoinactivation of Chinese Hamster Cells. *Cancer Res.* **1985**, *45*, 2008–2011.
18. Hockel, M.; Vaupel, P. Tumor Hypoxia: Definitions and Current Clinical, Biologic, and Molecular Aspects. *J. Natl. Cancer Inst.* **2001**, *93*, 266–276.
19. Chapman, J. D.; McPhee, M. S.; Walz, N.; Chetner, M. P.; Stobbe, C. C.; Soderlind, K.; Arnfield, M.; Meeker, B. E.; Trimble, L.; Allen, P. S. Nuclear Magnetic Resonance Spectroscopy and Sensitizer-Adduct Measurements of Photodynamic Therapy-Induced Ischemia in Solid Tumors. *J. Natl. Cancer Inst.* **1991**, *83*, 1650–1659.
20. Boulnois, J.-L. Photophysical Processes in Recent Medical Laser Developments: A Review. *Lasers Med. Sci.* **1986**, *1*, 47–66.
21. Nikfarjam, M.; Muralidharan, V.; Christophi, C. Mechanisms of Focal Heat Destruction of Liver Tumors. *J. Surg. Res.* **2005**, *127*, 208–223.
22. Chen, J.; Wang, D.; Xi, J.; Au, L.; Siekkinen, A.; Warsen, A.; Li, Z. Y.; Zhang, H.; Xia, Y.; Li, X. Immuno Gold Nanocages with Tailored Optical Properties for Targeted Photothermal Destruction of Cancer Cells. *Nano Lett.* **2007**, *7*, 1318–1322.
23. Chen, J.; Glaus, C.; Laforest, R.; Zhang, Q.; Yang, M.; Gidding, M.; Welch, M. J.; Xia, Y. Gold Nanocages as Photothermal Transducers for Cancer Treatment. *Small* **2010**, *6*, 811–817.
24. Cobley, C. M.; Au, L.; Chen, J.; Xia, Y. Targeting Gold Nanocages to Cancer Cells for Photothermal Destruction and Drug Delivery. *Expert Opin. Drug Delivery* **2010**, *7*, 577–587.
25. Dickerson, E. B.; Dreaden, E. C.; Huang, X.; El-Sayed, I. H.; Chu, H.; Pushpanketh, S.; McDonald, J. F.; El-Sayed, M. A. Gold Nanorod Assisted Near-Infrared Plasmonic Photothermal Therapy (PPTT) of Squamous Cell Carcinoma in Mice. *Cancer Lett.* **2008**, *269*, 57–66.
26. von Maltzahn, G.; Park, J. H.; Agrawal, A.; Bandaru, N. K.; Das, S. K.; Sailor, M. J.; Bhatia, S. N. Computationally Guided Photothermal Tumor Therapy Using Long-Circulating Gold Nanorod Antennas. *Cancer Res.* **2009**, *69*, 3892–3900.
27. Melancon, M. P.; Lu, W.; Yang, Z.; Zhang, R.; Cheng, Z.; Elliot, A. M.; Stafford, J.; Olson, T.; Zhang, J. Z.; Li, C. *In Vitro* and *In Vivo* Targeting of Hollow Gold Nanoshells Directed at Epidermal Growth Factor Receptor for Photothermal Ablation Therapy. *Mol. Cancer Ther.* **2008**, *7*, 1730–1739.

28. Carpin, L. B.; Bickford, L. R.; Agollah, G.; Yu, T. K.; Schiff, R.; Li, Y.; Drezek, R. A. Immunoconjugated Gold Nanoshell-Mediated Photothermal Ablation of Trastuzumab-Resistant Breast Cancer Cells. *Breast Cancer Res. Treat.* **2011**, *125*, 27–34.
29. Huang, X.; Qian, W.; El-Sayed, I. H.; El-Sayed, M. A. The Potential Use of the Enhanced Nonlinear Properties of Gold Nanospheres in Photothermal Cancer Therapy. *Lasers Surg. Med.* **2007**, *39*, 747–753.
30. Lu, W.; Melancon, M. P.; Xiong, C.; Huang, Q.; Elliott, A.; Song, S.; Zhang, R.; Flores, L. G., II; Gelovani, J. G.; Wang, L. V.; *et al.* Effects of Photoacoustic Imaging and Photothermal Ablation Therapy Mediated by Targeted Hollow Gold Nanospheres in an Orthotopic Mouse Xenograft Model of Glioma. *Cancer Res.* **2011**, *71*, 6116–6121.
31. Chakravarty, P.; Marches, R.; Zimmerman, N. S.; Swafford, A. D.; Bajaj, P.; Musselman, I. H.; Pantano, P.; Draper, R. K.; Vitetta, E. S. Thermal Ablation of Tumor Cells with Antibody-Functionalized Single-Walled Carbon Nanotubes. *Proc. Natl. Acad. Sci. U.S.A.* **2008**, *105*, 8697–8702.
32. Moon, H. K.; Lee, S. H.; Choi, H. C. *In Vivo* Near-Infrared Mediated Tumor Destruction by Photothermal Effect of Carbon Nanotubes. *ACS Nano* **2009**, *3*, 3707–3713.
33. Murakami, T.; Nakatsuji, H.; Inada, M.; Matoba, Y.; Umeyama, T.; Tsujimoto, M.; Isoda, S.; Hashida, M.; Imahori, H. Photodynamic and Photothermal Effects of Semiconducting and Metallic-Enriched Single-Walled Carbon Nanotubes. *J. Am. Chem. Soc.* **2012**, *134*, 17862–17865.
34. Wang, L.; Shi, J.; Zhang, H.; Li, H.; Gao, Y.; Wang, Z.; Wang, H.; Li, L.; Zhang, C.; Chen, C.; *et al.* Synergistic Anticancer Effect of Rnai and Photothermal Therapy Mediated by Functionalized Single-Walled Carbon Nanotubes. *Biomaterials* **2013**, *34*, 262–274.
35. O'Connell, M. J.; Bachilo, S. M.; Huffman, C. B.; Moore, V. C.; Strano, M. S.; Haroz, E. H.; Rialon, K. L.; Boul, P. J.; Noon, W. H.; Kittrell, C.; *et al.* Band Gap Fluorescence from Individual Single-Walled Carbon Nanotubes. *Science* **2002**, *297*, 593–596.
36. Huang, X.; Jain, P. K.; El-Sayed, I. H.; El-Sayed, M. A. Plasmonic Photothermal Therapy (PPTT) Using Gold Nanoparticles. *Lasers Med. Sci.* **2008**, *23*, 217–228.
37. Jori, G.; Spikes, J. D. Photothermal Sensitizers: Possible Use in Tumor Therapy. *J. Photochem. Photobiol. B* **1990**, *6*, 93–101.
38. Anderson, R. R.; Parrish, J. A. Selective Photothermolysis: Precise Microsurgery by Selective Absorption of Pulsed Radiation. *Science* **1983**, *220*, 524–527.
39. Chen, W. R.; Adams, R. L.; Bartels, K. E.; Nordquist, R. E. Chromophore-Enhanced *In Vivo* Tumor Cell Destruction Using an 808-nm Diode Laser. *Cancer Lett.* **1995**, *94*, 125–131.
40. Jay, D. G. Selective Destruction of Protein Function by Chromophore-Assisted Laser Inactivation. *Proc. Natl. Acad. Sci. U.S.A.* **1988**, *85*, 5454–5458.
41. Chen, W. R.; Adams, R. L.; Higgins, A. K.; Bartels, K. E.; Nordquist, R. E. Photothermal Effects on Murine Mammary Tumors Using Indocyanine Green and an 808-nm Diode Laser: An *In Vivo* Efficacy Study. *Cancer Lett.* **1996**, *98*, 169–173.
42. Yu, J.; Javier, D.; Yaseen, M. A.; Nitin, N.; Richards-Kortum, R.; Anvari, B.; Wong, M. S. Self-Assembly Synthesis, Tumor Cell Targeting, and Photothermal Capabilities of Antibody-Coated Indocyanine Green Nanocapsules. *J. Am. Chem. Soc.* **2010**, *132*, 1929–1938.
43. Camerin, M.; Rello, S.; Villanueva, A.; Ping, X.; Kenney, M. E.; Rodgers, M. A.; Jori, G. Photothermal Sensitisation as a Novel Therapeutic Approach for Tumours: Studies at the Cellular and Animal Level. *Eur. J. Cancer* **2005**, *41*, 1203–1212.
44. Busetti, A.; Soncin, M.; Reddi, E.; Rodgers, M. A.; Kenney, M. E.; Jori, G. Photothermal Sensitization of Amelanotic Melanoma Cells by Ni(II)-Octabutoxy-Naphthalocyanine. *J. Photochem. Photobiol. B* **1999**, *53*, 103–109.
45. Soncin, M.; Busetti, A.; Fusi, F.; Jori, G.; Rodgers, M. A. Irradiation of Amelanotic Melanoma Cells with 532 nm High Peak Power Pulsed Laser Radiation in the Presence of the Photothermal Sensitizer Cu(II)-Hematoporphyrin: A New Approach to Cell Photoinactivation. *Photochem. Photobiol.* **1999**, *69*, 708–712.
46. Yguerabide, J.; Yguerabide, E. E. Light-Scattering Submicroscopic Particles as Highly Fluorescent Analogs and Their Use as Tracer Labels in Clinical and Biological Applications. *Anal. Biochem.* **1998**, *262*, 137–156.
47. Kanehara, M.; Takahashi, H.; Teranishi, T. Gold(0) Porphyrins on Gold Nanoparticles. *Angew. Chem., Int. Ed.* **2008**, *47*, 307–310.
48. Baskaran, D.; Mays, J. W.; Zhang, X. P.; Bratcher, M. S. Carbon Nanotubes with Covalently Linked Porphyrin Antennae: Photoinduced Electron Transfer. *J. Am. Chem. Soc.* **2005**, *127*, 6916–6917.
49. Jang, B.; Park, J. Y.; Tung, C. H.; Kim, I. H.; Choi, Y. Gold Nanorod-Photosensitizer Complex for Near-Infrared Fluorescence Imaging and Photodynamic/Photothermal Therapy *in Vivo*. *ACS Nano* **2011**, *5*, 1086–1094.
50. Lovell, J. F.; Jin, C. S.; Huynh, E.; Jin, H.; Kim, C.; Rubinstein, J. L.; Chan, W. C.; Cao, W.; Wang, L. V.; Zheng, G. Porphysome Nanovesicles Generated by Porphyrin Bilayers for Use as Multimodal Biophotonic Contrast Agents. *Nat. Mater.* **2011**, *10*, 324–332.
51. Lovell, J. F.; Jin, C. S.; Huynh, E.; MacDonald, T. D.; Cao, W.; Zheng, G. Enzymatic Regioselection for the Synthesis and Biodegradation of Porphysome Nanovesicles. *Angew. Chem., Int. Ed.* **2012**, *51*, 2429–2433.
52. Wang, G. L.; Jiang, B. H.; Rue, E. A.; Semenza, G. L. Hypoxia-Inducible Factor 1 Is a Basic-Helix-Loop-Helix-Pas Heterodimer Regulated by Cellular O2 Tension. *Proc. Natl. Acad. Sci. U.S.A.* **1995**, *92*, 5510–5514.
53. O'Neal, D. P.; Hirsch, L. R.; Halas, N. J.; Payne, J. D.; West, J. L. Photo-thermal Tumor Ablation in Mice Using Near Infrared-Absorbing Nanoparticles. *Cancer Lett.* **2004**, *209*, 171–176.
54. Camerin, M.; Rodgers, M. A.; Kenney, M. E.; Jori, G. Photothermal Sensitisation: Evidence for the Lack of Oxygen Effect on the Photosensitising Activity. *Photochem. Photobiol. Sci* **2005**, *4*, 251–253.
55. Wheatley, D. N.; Kerr, C.; Gregory, D. W. Heat-Induced Damage to HeLa-S3 Cells: Correlation of Viability, Permeability, Osmosensitivity, Phase-Contrast Light-, Scanning Electron- and Transmission Electron-Microscopical Findings. *Int. J. Hyperthermia* **1989**, *5*, 145–162.
56. Liu, T. W.; MacDonald, T. D.; Shi, J.; Wilson, B. C.; Zheng, G. Intrinsically Copper-64-Labeled Organic Nanoparticles as Radiotracers. *Angew. Chem.* **2012**, *51*, 13128–13131.